

**Deterioration of the piezoelectric properties of  $(\text{Bi}_{0.5}\text{Na}_{0.5})\text{TiO}_3$  when using  $\text{Na}_2\text{CO}_3$  as a sintering aid**

**A crystallographic and microstructural study**

Mahon, Tadhg; Giannopoulos, Dimosthenis; van der Zwaag, Sybrand; Groen, Pim

**DOI**

[10.1063/5.0044636](https://doi.org/10.1063/5.0044636)

**Publication date**

2021

**Document Version**

Final published version

**Published in**

Journal of Applied Physics

**Citation (APA)**

Mahon, T., Giannopoulos, D., van der Zwaag, S., & Groen, P. (2021). Deterioration of the piezoelectric properties of  $(\text{Bi}_{0.5}\text{Na}_{0.5})\text{TiO}_3$  when using  $\text{Na}_2\text{CO}_3$  as a sintering aid: A crystallographic and microstructural study. *Journal of Applied Physics*, 129(13), Article 134102. <https://doi.org/10.1063/5.0044636>

**Important note**

To cite this publication, please use the final published version (if applicable). Please check the document version above.

**Copyright**

Other than for strictly personal use, it is not permitted to download, forward or distribute the text or part of it, without the consent of the author(s) and/or copyright holder(s), unless the work is under an open content license such as Creative Commons.

**Takedown policy**

Please contact us and provide details if you believe this document breaches copyrights. We will remove access to the work immediately and investigate your claim.

***Green Open Access added to TU Delft Institutional Repository***

***'You share, we take care!' - Taverne project***

**<https://www.openaccess.nl/en/you-share-we-take-care>**

Otherwise as indicated in the copyright section: the publisher is the copyright holder of this work and the author uses the Dutch legislation to make this work public.

# Deterioration of the piezoelectric properties of $(\text{Bi}_{0.5}\text{Na}_{0.5})\text{TiO}_3$ when using $\text{Na}_2\text{CO}_3$ as a sintering aid: A crystallographic and microstructural study

Cite as: J. Appl. Phys. 129, 134102 (2021); <https://doi.org/10.1063/5.0044636>

Submitted: 18 January 2021 . Accepted: 15 March 2021 . Published Online: 06 April 2021

 Tadhg Mahon,  Dimosthenis Giannopoulos,  Sybrand van der Zwaag, and  Pim Groen



View Online



Export Citation



CrossMark

## ARTICLES YOU MAY BE INTERESTED IN

[Enhanced multiferroic characteristics in hexagonal  \$\text{ScMn}\_{1-x}\text{Fe}\_x\text{O}\_3\$  ceramics](#)

Journal of Applied Physics 129, 134101 (2021); <https://doi.org/10.1063/5.0040475>

[Acoustic levitation of a Mie sphere using a 2D transducer array](#)

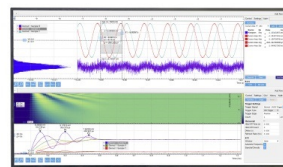
Journal of Applied Physics 129, 134901 (2021); <https://doi.org/10.1063/5.0037344>

[Localization of ultrasound in 2D phononic crystal with randomly oriented asymmetric scatterers](#)

Journal of Applied Physics 129, 134701 (2021); <https://doi.org/10.1063/5.0041659>

Challenge us.

What are your needs for  
periodic signal detection?



Zurich  
Instruments

# Deterioration of the piezoelectric properties of $(\text{Bi}_{0.5}\text{Na}_{0.5})\text{TiO}_3$ when using $\text{Na}_2\text{CO}_3$ as a sintering aid: A crystallographic and microstructural study

Cite as: J. Appl. Phys. **129**, 134102 (2021); doi: [10.1063/5.0044636](https://doi.org/10.1063/5.0044636)

Submitted: 18 January 2021 · Accepted: 15 March 2021 ·

Published Online: 6 April 2021



Tadhg Mahon,<sup>a)</sup> Dimosthenis Giannopoulos, Sybrand van der Zwaag, and Pim Groen<sup>b)</sup>

## AFFILIATIONS

Novel Aerospace Materials (NovAM) group, Faculty of Aerospace Engineering, Technical University of Delft

<sup>a)</sup>Author to whom correspondence should be addressed: [t.r.mahon@tudelft.nl](mailto:t.r.mahon@tudelft.nl) and [tadghmahon2@gmail.com](mailto:tadghmahon2@gmail.com)

<sup>b)</sup>Deceased.

## ABSTRACT

In this work, we present the impact of using  $\text{Na}_2\text{CO}_3$  as a sintering aid and grain growth agent on the crystal structure, microstructure, and piezoelectric properties of  $(\text{Bi}_{0.5}\text{Na}_{0.5})\text{TiO}_3$  ceramics. The addition of  $\text{Na}_2\text{CO}_3$  leads to a substantial increase in the grain size and density even at a reduced sintering temperature of 1025 °C. However, at the same time, the value of the piezoelectric constant  $d_{33}$  drops dramatically. Using high-resolution x-ray diffraction analysis, we demonstrate that the decrease in piezoelectric constant is due to a change in the chemical composition of the  $(\text{Bi}_{0.5}\text{Na}_{0.5})\text{TiO}_3$  base material rather than due to the change in the grain size. High  $\text{Na}_2\text{CO}_3$ -addition levels lead to the formation of  $\text{Bi}_2\text{O}_3$  as a secondary phase during sintering too.

Published under license by AIP Publishing. <https://doi.org/10.1063/5.0044636>

## I. INTRODUCTION

Piezoelectric ceramics are a useful subset of electroceramics that can be used for motors,<sup>1</sup> actuators,<sup>2–5</sup> ultrasonic transducers,<sup>5,6</sup> sensors,<sup>5,7</sup> and energy harvesting applications<sup>8</sup> through their coupling of the mechanical and electrical energy domains. Currently, commercial piezoelectric ceramics rely heavily on lead zirconium titanate (PZT). Due to the high concentration of lead, these ceramics present some concerns for human and environmental health. The use of lead in electronic applications has already been significantly restricted by the European Union Directive on the Restriction of Hazardous Substances in Electrical and Electronic Equipment (RoHS2)<sup>5,9</sup> with some exceptions made for piezoelectric applications due to the lack of an available substitute. While a number of prospective lead-free ceramics, such as  $(\text{Bi}_{0.5}\text{Na}_{0.5})\text{TiO}_3$  based and  $(\text{K}_{0.5}\text{Na}_{0.5})\text{NbO}_3$  based systems,<sup>5,10–14</sup> have been identified as possible replacements for PZT, these systems face a number of problems that prevent them from entering into widespread use. One such problem is the presence of volatile elements in these ceramics that can generate off-stoichiometry during the sintering process, especially in  $(\text{Bi}_{0.5}\text{Na}_{0.5})\text{TiO}_3$ .<sup>15</sup> This change in the composition can negatively impact the piezoelectric properties of the final ceramic. One solution to this is to use cold or fast sintering

methods such as spark plasma sintering (SPS);<sup>16,17</sup> however, this technique is not scalable to industrial levels. An alternative option is to incorporate a sintering aid to reduce the sintering temperature of the ceramic and so avoid the high temperatures where volatilization becomes a problem. Sintering aids are additives that increase the speed of sintering, often by the introduction of a liquid phase at a temperature below the normal sintering temperature.<sup>18</sup> A number of studies have been carried out on the inclusion of sintering aids in  $(\text{Bi}_{0.5}\text{Na}_{0.5})\text{TiO}_3$  such as  $\text{CuO}$ ,<sup>19</sup>  $\text{MgO}$ ,<sup>20</sup> or  $\text{Fe}_2\text{O}_3$ .<sup>21,22</sup> The addition of each of these sintering aids allowed access to higher densities at lower temperatures with  $\text{CuO}$  lowering the required sintering temperature from 1075–1100 °C<sup>22</sup> to 950 °C,  $\text{MgO}$  lowering it to 1000 °C, and  $\text{Fe}_2\text{O}_3$  to 900 °C. While sintering aids can be a valuable tool in the creation of dense ceramics at lower sintering temperatures, the introduction of this second phase during the sintering process may lead to interactions with the crystal structure (doping, leaching or substitution) such as that observed by Zhao *et al.* who included  $\text{B}_2\text{O}_3$  with a  $\text{CuO}$  sintering aid for a modified  $\text{BaTiO}_3$  ceramic, which had a favorable impact on the properties.<sup>23</sup> In this work, we will present a study on the use of  $\text{Na}_2\text{CO}_3$  as a sintering aid to produce dense  $(\text{Bi}_{0.5}\text{Na}_{0.5})\text{TiO}_3$  ceramics at a lower temperature than what is used for bulk

$(\text{Bi}_{0.5}\text{Na}_{0.5})\text{TiO}_3$  production without the use of a sintering aid. We will discuss the interaction of the sintering aid with the crystal structure and demonstrate how this leads to a deterioration of the piezoelectric properties of the final ceramics as well as the changes observed in the microstructure of the ceramic.

## II. EXPERIMENTAL

$(\text{Bi}_{0.5}\text{Na}_{0.5})\text{TiO}_3$  was obtained from PI ceramics in the form of loose powder with an approximate particle size of 250 nm. This powder was mixed with 0, 0.1, 1, and 3 wt. % sodium carbonate by hand-milling in hexane for 20 min to ensure good mixing. The powder was cold pressed into pellets of 10 mm diameter before being sintered for 2 h at 1025 °C in alumina crucibles on a small layer of powder, of the same composition. The density of the pellets was measured using the Archimedes method before gold electrodes were sputtered onto the ceramic discs using a Quorum Q300 T sputter coater. The phase purity and crystal structures of the starting powder and the pellets were checked by XRD. One pellet from each composition was ground to produce a powder for analysis. High-resolution x-ray diffraction (XRD) was performed using a Bruker D8 Advanced diffractometer with  $\text{Co K}\alpha$  source [ $K\alpha_1(100) = 1.78900 \text{ \AA}$ ,  $K\alpha_2(50) = 1.79283 \text{ \AA}$ ] and a Lynxeye position sensitive detector. A step size of 0.002 was employed and measurements were taken between  $2\theta = 20^\circ$  and  $90^\circ$  with the Bragg-Brentano geometry. For the off-stoichiometric samples, lower resolution measurements were taken using a Rigaku MiniFlex 600 tabletop diffractometer and  $\text{Cu K}\alpha$  radiation with a step size of  $0.01^\circ$  and  $\theta-2\theta$  configuration. Scanning Electron Microscope (SEM) images and energy dispersive x-ray spectroscopy (EDX)

were taken using a Jeol JSM-7500F field emission scanning electron microscope. The grain size for the samples was measured by first polishing and then thermally etching at 1000 °C for 20 min to reveal the grain boundaries. Lower etching temperatures were initially attempted but did not result in observable grain boundaries. The interior morphology was also measured after polishing the samples for electrode deposition. Prior to SEM measurements, a thin (15 nm) layer of gold is deposited on the sample using the sputter coater described above. Grain size distribution analysis was performed on the SEM images using the imageJ software to isolate, count, and measure each grain. Magnifications were chosen such that a large number of grains were clearly visible, and for the 1 and 3 wt. % samples, three separate images were combined to provide good measurement statistics. The ceramic discs were poled using contact poling in a bath of silicone oil at 100 °C and an applied field of 4 kV/mm for 20 min. The electrical properties of the discs were measured at room temperature using an Agilent 4263B LCR meter at 1 kHz and 1 V, while the piezoelectric properties were measured using a PM300 Berlincourt-type piezometer from Piezotest with a static force of 10 N and a dynamic force of 0.25 N peak to peak with sinusoidal excitation at 110 Hz.

## III. RESULTS AND DISCUSSION

### A. Stoichiometric $(\text{Bi}_{0.5}\text{Na}_{0.5})\text{TiO}_3$

#### 1. XRD

The XRD patterns on the  $(\text{Bi}_{0.5}\text{Na}_{0.5})\text{TiO}_3$  pellets with  $x$  wt. % additional  $\text{Na}_2\text{CO}_3$  ( $0 \leq x \leq 3$ ) added during sintering as a grain growth agent are presented in Fig. 1(a). XRD indicates that the

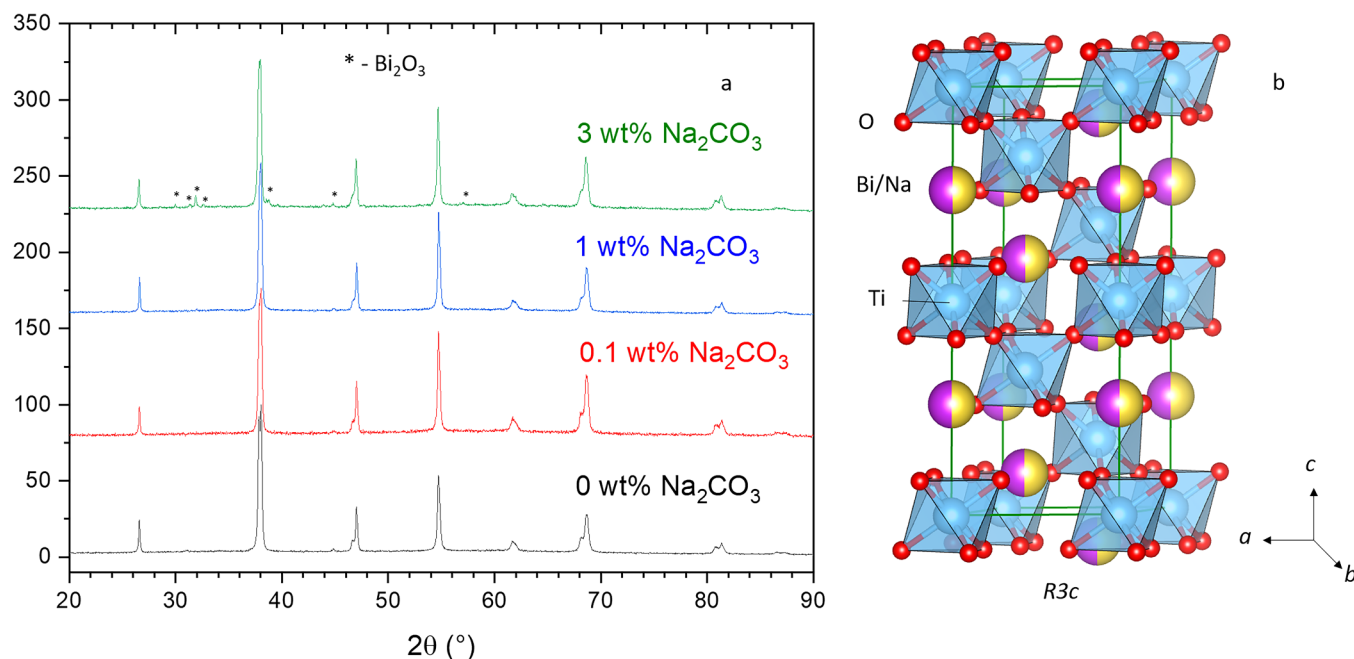
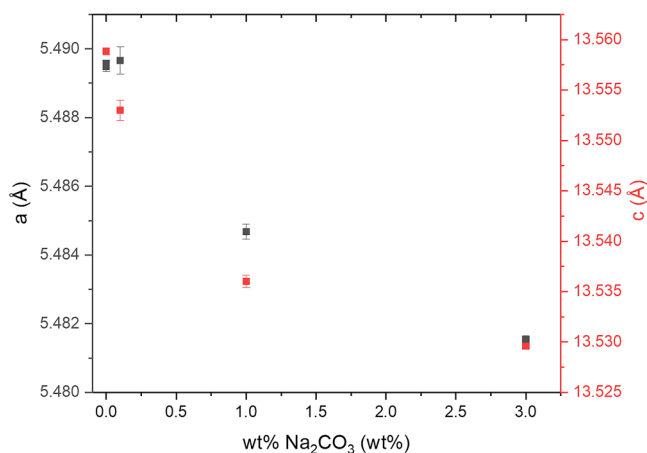


FIG. 1. (a) XRD patterns of  $(\text{Bi}_{0.5}\text{Na}_{0.5})\text{TiO}_3$  after sintering at 1025 °C with  $\text{Na}_2\text{CO}_3$ , (b) hexagonal representation of the crystal structure of  $(\text{Bi}_{0.5}\text{Na}_{0.5})\text{TiO}_3$ .



**FIG. 2.** Plot of the  $a$  and  $c$  unit cell parameters of  $(\text{Bi}_{0.5}\text{Na}_{0.5})\text{TiO}_3$  against the amount of  $\text{Na}_2\text{CO}_3$  sintering aid added.

samples are single phase, rhombohedral,  $(\text{Bi}_{0.5}\text{Na}_{0.5})\text{TiO}_3$  with no apparent secondary phases apart from the sample with 3 wt. % additional  $\text{Na}_2\text{CO}_3$  where several peaks corresponding to a  $\text{Bi}_2\text{O}_3$  secondary phase are observed. The actual crystal structure of  $(\text{Bi}_{0.5}\text{Na}_{0.5})\text{TiO}_3$  is presented in Fig. 1(b).

A decrease in the unit cell parameters is observed with increasing the  $\text{Na}_2\text{CO}_3$  content as depicted in Fig. 2. The unit cell parameters of pristine (no sintering aid)  $(\text{Bi}_{0.5}\text{Na}_{0.5})\text{TiO}_3$  are  $a = 5.4896(1)$  Å and  $c = 13.5588(3)$  Å, which is in reasonably good agreement with the structure found by Jones *et al.*,<sup>24</sup> although the  $c$  parameter is larger than their observed value [ $a = 5.4887(2)$  and  $c = 13.5048$  Å]. The origin of this deviation is likely due to increased loss of volatile elements from the significantly longer calcination time (12 h vs 2 h for this work) used by Jones *et al.* and the higher temperature of 1075 °C (compared to 1025 °C in this study). It should also be noted that, while no off-stoichiometry due to volatilization was detected for our samples, it cannot be completely ruled out that small off-stoichiometries are caused during the calcination/sintering processes and so the actual compositions of our samples may be slightly different than the nominal. However, as the sintering temperature was kept constant for all samples, any possible volatilization cannot explain the reduction in the unit cell parameters with increasing  $\text{Na}_2\text{CO}_3$  loadings. The decrease observed in the unit cell parameters with increasing levels

**TABLE I.** Summary of the Rietveld refinement on pellets of  $(\text{Bi}_{0.5}\text{Na}_{0.5})\text{TiO}_3$  with different amounts of sintering aid added.

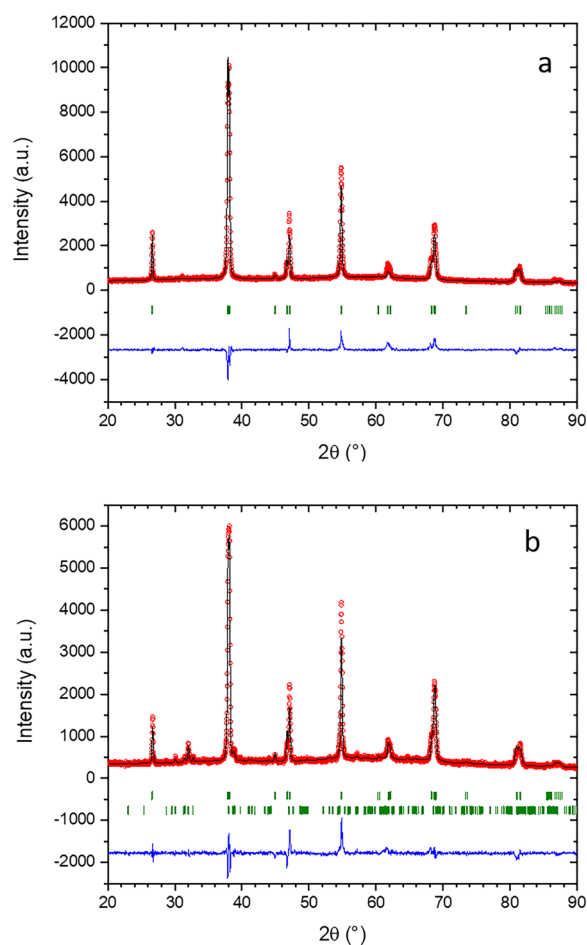
	0 wt. % $\text{Na}_2\text{CO}_3$	3 wt. % $\text{Na}_2\text{CO}_3$	$\Delta$ (%)
$a$ (Å)	5.4896(1)	5.4816(1)	-0.15
$c$ (Å)	13.5588(3)	13.5296(2)	-0.22
$V$ (Å <sup>3</sup> )	353.861	352.071	-0.51
R-Bragg	5.71	9.84	

**TABLE II.** Refined crystal structure of  $(\text{Bi}_{0.5}\text{Na}_{0.5})\text{TiO}_3$  sintered at 1025 °C with (top) no added sintering aid and (bottom) 3 wt. %  $\text{Na}_2\text{CO}_3$  sintering aid. Occupancies account for site multiplicity.

Atom	x	y	z	$B_{\text{iso}}$	Occupancy
Na	0	0	0.267(5)	3.83(6)	0.5
Bi	0	0	0.267(5)	3.83(6)	0.5
Ti	0	0	0.0025(4)	2.22(8)	1.00
O	0.128(2)	0.321(2)	0.086(2)	2.22(8)	3.00

Atom	x	y	z	$B_{\text{iso}}$	Occupancy
Na	0	0	0.268(3)	3.323(8)	0.53(1)
Bi	0	0	0.268(3)	3.323(8)	0.47(1)
Ti	0	0	0.0037(7)	0.87(9)	1.00
O	0.130(6)	0.287(3)	0.111(1)	0.87(9)	2.97(1)



**FIG. 3.** Rietveld refinements of the XRD patterns for  $(\text{Bi}_{0.5}\text{Na}_{0.5})\text{TiO}_3$  sintered with (a) no additional  $\text{Na}_2\text{CO}_3$  and (b) 3 wt. %  $\text{Na}_2\text{CO}_3$  added. In both cases, the upper row of ticks corresponds to the primary  $(\text{Bi}_{0.5}\text{Na}_{0.5})\text{TiO}_3$  phase and for refinement  $b$ , the lower ticks show the position of the peaks for  $\text{Bi}_2\text{O}_3$ .

of  $\text{Na}_2\text{CO}_3$  is thus indicative of substitution of bismuth by the smaller sodium ions and a corresponding increase in oxygen vacancies in order to balance the charge. This is confirmed by the formation of  $\text{Bi}_2\text{O}_3$  at higher loadings. Bismuth can only have come from the principle phase and the absence of  $\text{Bi}_2\text{O}_3$  at lower loadings and in the stoichiometric sample rules out its precipitation as a response to Na volatilization alone.

Rietveld analysis was performed on pristine  $(\text{Bi}_{0.5}\text{Na}_{0.5})\text{TiO}_3$  and the sample with 3 wt. %  $\text{Na}_2\text{CO}_3$  sintering aid based on the structure of Jones *et al.*<sup>24</sup> as a starting point. The results of this refinement are summarized in Tables I and II and the refinements can be seen in Fig. 3. Addition of excess sodium causes a slight reduction in the unit cell volume of (−0.51%) with both the *a* and

the *c* parameters decreasing, consistent with insertion of Na ions into the structure in place of Bi ions. Rietveld analysis of the structures indicates the creation of oxygen vacancies to balance the charge in this new, off-stoichiometric  $(\text{Bi}_{0.5}\text{Na}_{0.5})\text{TiO}_3$  and tilting of the oxygen octahedra during this substitution. The refinement thus indicates that the composition of the  $(\text{Bi}_{0.5}\text{Na}_{0.5})\text{TiO}_3$  after the addition of 3 wt. %  $\text{Na}_2\text{CO}_3$  sintering aid is  $(\text{Bi}_{0.47}\text{Na}_{0.53})\text{TiO}_{2.97}$ . This compositional change toward a sodium rich phase is assumed to happen to a lesser extent in the samples with 0.1 and 1 wt. %  $\text{Na}_2\text{CO}_3$  that is too small to be accurately detected in these samples. Attempts were made to also observe the compositional changes through EDX, however, the equipment was not sensitive enough to detect any significant changes in the composition.

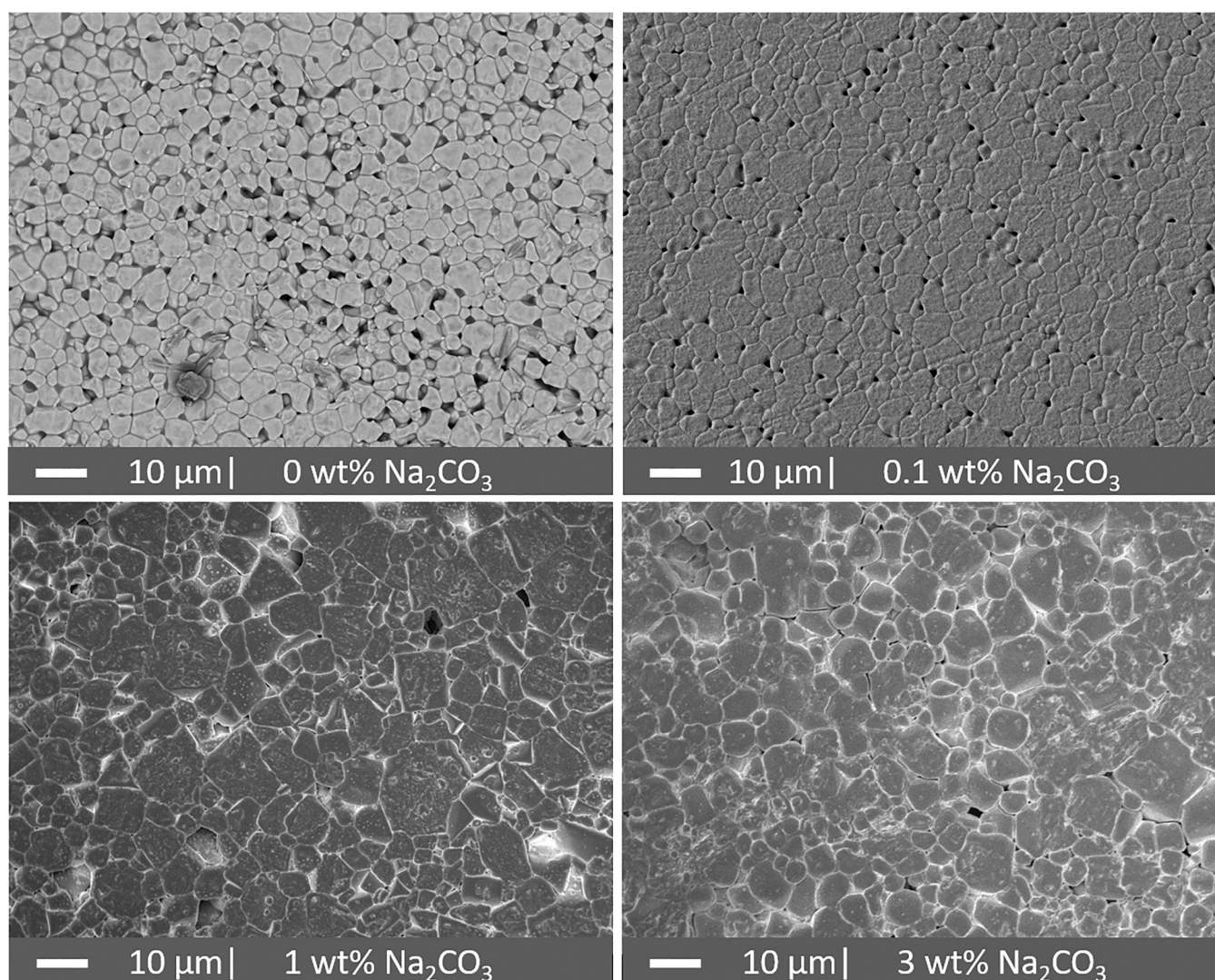


FIG. 4. SEM images of the etched  $(\text{Bi}_{0.5}\text{Na}_{0.5})\text{TiO}_3$  pellets after sintering at 1025 °C with 0, 0.1, 1, and 3 wt. % added  $\text{Na}_2\text{CO}_3$ .

## 2. Microstructure

SEM images were taken to analyse the microstructure of the  $(\text{Bi}_{0.5}\text{Na}_{0.5})\text{TiO}_3$  ceramics with different loadings of the  $\text{Na}_2\text{CO}_3$  sintering aid. A representative image of the microstructure for each etched sample is shown in Fig. 4, and the grain size distributions, calculated by image analysis from these surface images, are given in Fig. 5. When no  $\text{Na}_2\text{CO}_3$  is added, the chosen sintering temperature of  $1025^\circ\text{C}$  is, as expected, too low for complete densification, leading to visible porosity in the microstructure. The final ceramic consists of grains with tight size distribution and an average size of  $1.89\ \mu\text{m}$ . When  $0.1\ \text{wt}\%$   $\text{Na}_2\text{CO}_3$  is added, there is a marked increase in the grain size and a reduction in the porosity. Most of the grains lie between  $2$  and  $5\ \mu\text{m}$  with a small number of very large grains. The average grain size for this sample is  $3.03\ \mu\text{m}$ , significantly larger than the  $0\ \text{wt}\%$   $\text{Na}_2\text{CO}_3$  sample.

Once the loading of  $\text{Na}_2\text{CO}_3$  is increased to  $1\ \text{wt}\%$ , the densification of the pellet is visibly improved with most of the porosity disappearing. The grain size distribution moves slightly toward larger sizes with an average size of  $3.71\ \mu\text{m}$ . At this loading, small

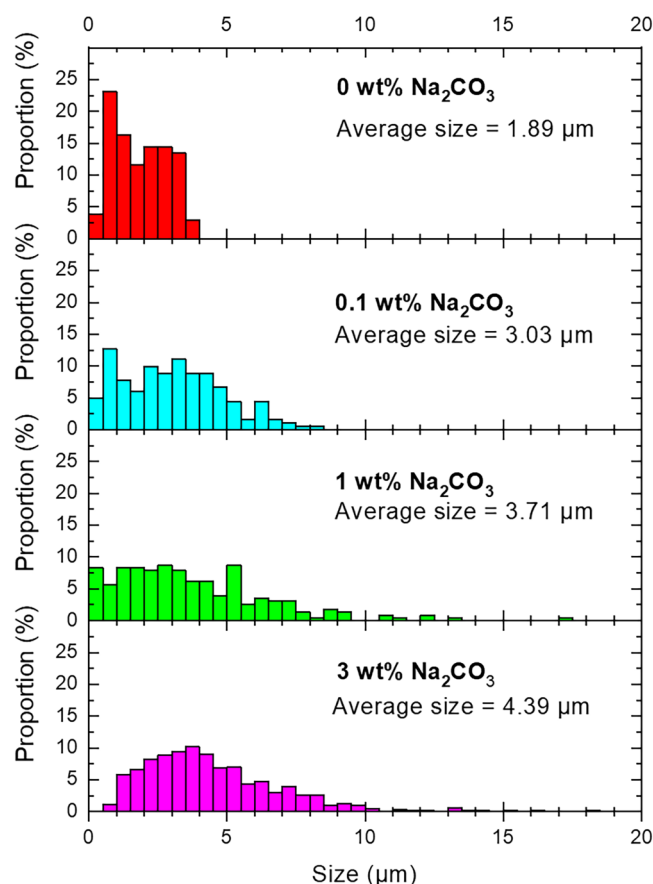


FIG. 5. Grain size distribution in the  $(\text{Bi}_{0.5}\text{Na}_{0.5})\text{TiO}_3$  pellets calculated from SEM images.

precipitates are visible at some of the grain boundaries. These are expected to be  $\text{Bi}_2\text{O}_3$  as seen in the XRD pattern of the highest loading, but due to their small size, their composition could not be reliably measured with EDX. When viewing the microstructure of the  $3\ \text{wt}\%$   $\text{Na}_2\text{CO}_3$  loaded sample, the presence of these precipitates is much clearer. The grain size distribution has further increased toward larger grain sizes with an average size of  $4.39\ \mu\text{m}$ . From these data, it can be concluded that  $\text{Na}_2\text{CO}_3$  acts as a sintering aid for  $(\text{Bi}_{0.5}\text{Na}_{0.5})\text{TiO}_3$  ceramics.

The XRD data also indicated the formation of  $\text{Bi}_2\text{O}_3$ , which was attributed to the displacement of Bi ions from the lattice by Na ions. Close inspection of the microstructure of the  $3\ \text{wt}\%$   $\text{Na}_2\text{CO}_3$  sample with SEM on a fracture surface indeed reveals the presence of a second phase in the intergranular spaces shown by the lighter shading in Fig. 6. Analysis of this phase by EDX confirms that it is  $\text{Bi}_2\text{O}_3$ , as observed in the XRD pattern of this sample in Fig. 1.

## 3. Piezoelectric and dielectric properties

The piezoelectric and dielectric properties of the  $(\text{Bi}_{0.5}\text{Na}_{0.5})\text{TiO}_3$  pellets for  $0$ – $3\ \text{wt}\%$   $\text{Na}_2\text{CO}_3$  are summarized in Table III. Pristine  $(\text{Bi}_{0.5}\text{Na}_{0.5})\text{TiO}_3$  exhibits a  $d_{33}$  of  $62.0\ \text{pC/N}$ , a value slightly below the value reported for bulk  $(\text{Bi}_{0.5}\text{Na}_{0.5})\text{TiO}_3$  by Hiruma *et al.* of  $69.8\ \text{pC/N}$ .<sup>25</sup> The small difference between our observed value and the reported value is easily explained by differences in the density of our pristine sample ( $89.2\%$ ) vs the sample of Hiruma *et al.* ( $98.6\%$ ) who used a higher sintering temperature, more appropriate for the synthesis of bulk  $(\text{Bi}_{0.5}\text{Na}_{0.5})\text{TiO}_3$  in the absence of a sintering aid. Considering this difference in the density, the pristine sample displays a  $d_{33}$  value largely consistent with the literature. From the data in Table III, it can be seen that increasing the loading of  $\text{Na}_2\text{CO}_3$  (and thus the grain size) has a deleterious effect on the  $d_{33}$  of the ceramics with the  $d_{33}$  dropping

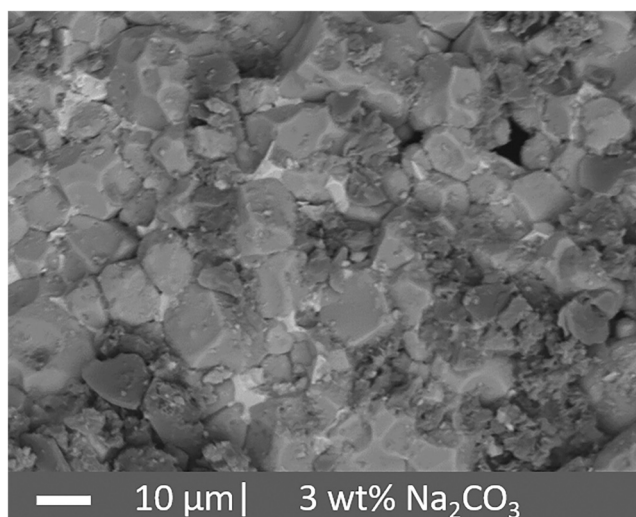


FIG. 6. Backscattered electron SEM image of a fracture surface of  $(\text{Bi}_{0.5}\text{Na}_{0.5})\text{TiO}_3$  with  $3\ \text{wt}\%$   $\text{Na}_2\text{CO}_3$ .

**TABLE III.** Summary of the piezoelectric and dielectric properties of  $(\text{Bi}_{0.5}\text{Na}_{0.5})\text{TiO}_3$  samples with varying levels of  $\text{Na}_2\text{CO}_3$ .

Wt. % $\text{Na}_2\text{CO}_3$	$\epsilon_r$	$\tan \delta$	$d_{33}$ (pC/N)	Relative density (%)
0	385	0.02	62.0	89.2
0.1	401	0.02	31.8	97.5
1	304	0.02	6.3	82.0
3	568	0.75	11.4	93.1

from 62.0 pC/N in the pristine sample to 6.3–11.4 pC/N in the sample with 1 and 3 wt. % loadings of  $\text{Na}_2\text{CO}_3$ , respectively, while the other properties remain largely unchanged. A maximum in the density (97.5%) is observed when only 0.1 wt. %  $\text{Na}_2\text{CO}_3$  is added, achieved at a sintering temperature of only 1025 °C. Therefore, a dramatic improvement in the densification of the  $(\text{Bi}_{0.5}\text{Na}_{0.5})\text{TiO}_3$  pellets can be achieved at temperatures below those typically employed for  $(\text{Bi}_{0.5}\text{Na}_{0.5})\text{TiO}_3$  ceramics. For example, Hiruma *et al.* employed hot pressing methods at 1080 °C<sup>26</sup> Kornpom *et al.* and Spreitzer *et al.* sintered at 1100–1150 °C.<sup>27,28</sup> However, while  $\text{Na}_2\text{CO}_3$  addition did indeed allow for a lower sintering temperature to be used, it was not as efficient as other sintering aids such as CuO, which reduces the sintering temperature to 950 °C.<sup>19</sup> Moreover, while low loadings of  $\text{Na}_2\text{CO}_3$  did improve the density, they led to a notable reduction in  $d_{33}$  from 62 to 31.8 pC/N. Above 0.1 wt. %  $\text{Na}_2\text{CO}_3$  loading, a decrease in the density is seen initially at 1 wt. % loading and then another increase at 3 wt. %, where  $\text{Bi}_2\text{O}_3$  precipitation improved the overall density. Unfortunately, this increase in density comes at the expense of the piezoelectric properties, which could be caused by two phenomena. First, it may

be due to the increase in the grain size, a well-studied phenomenon in  $\text{BaTiO}_3$  piezoceramics whereby the proportion of 90° domain walls increases as the grain size increases, progressively blocking polarization by preventing the domain wall movement.<sup>29,30</sup> Alternatively, the reduction in the properties could be due to the compositional changes such as those observed in the sample with the highest  $\text{Na}_2\text{CO}_3$  loading. Evidence for this compositional change is seen in the changing unit cell parameters at lower loadings, but the magnitude of the compositional changes is too small to be identified by other means such as the precipitation of  $\text{Bi}_2\text{O}_3$  in these samples. The observed dielectric constants ( $\epsilon_r$ ) of the samples are consistent with the expected value of around 380 seen in the literature<sup>31</sup> for all samples with the exception of the 3 wt. %  $\text{Na}_2\text{CO}_3$  sample. However, given the exceptionally high  $\tan \delta$  of this sample, it is difficult to reliably measure its real  $\epsilon_r$ .

This clearly raises the question of whether the reduction in the piezoelectric properties is due to the changes observed in the composition or the increase in the grain size. As these properties are coupled through the addition of  $\text{Na}_2\text{CO}_3$ , efforts must be made to deconvolute these two parameters. Figure 7 shows a plot of  $d_{33}$  against the  $\text{Na}_2\text{CO}_3$  loading (a) and the average grain size (b). Rapid decay is observed in  $d_{33}$  when adding  $\text{Na}_2\text{CO}_3$  while a linear decay is observed when considering the grain size.

To separate the effects of the grain size and composition on the piezoelectric properties, a sample with composition  $(\text{Bi}_{0.47}\text{Na}_{0.53})\text{TiO}_{2.97}$  was prepared using the same conditions as the other samples. This corresponds to the refined composition of the 3 wt. %  $\text{Na}_2\text{CO}_3$  sample from Table I. While this sample will be discussed in more detail in Sec. III B, it is instructive to also consider it here in comparison to the samples with  $\text{Na}_2\text{CO}_3$  grain growth agent added, as this sample did not exhibit any noticeable grain growth. In Fig. 7(a), the

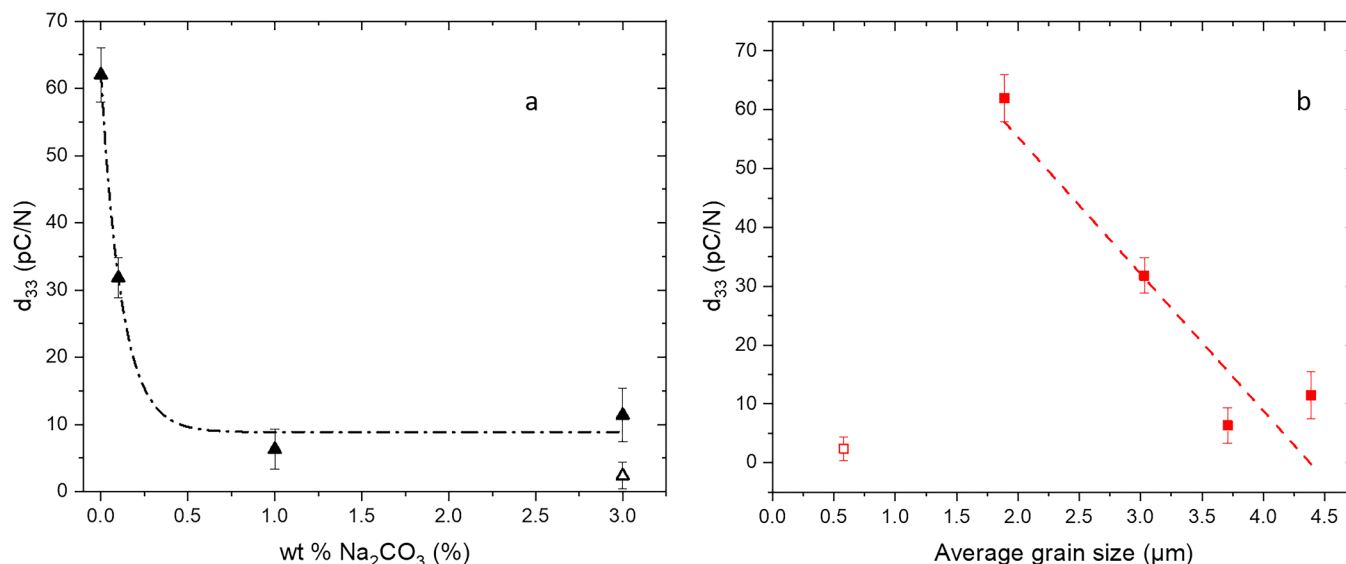


**FIG. 7.**  $d_{33}$  values of sintered samples vs (a)  $\text{Na}_2\text{CO}_3$  loading and (b) average grain size. The hollow point represents the Na-rich  $(\text{Bi}_{0.47}\text{Na}_{0.53})\text{TiO}_{2.97}$  sample. The dotted lines represent a fit using an exponential and linear decay function, respectively, and are added to illustrate the trends.

$d_{33}$  shows an exponential decrease with the addition of  $\text{Na}_2\text{CO}_3$  reaching a plateau around 0.5 wt.%. The hollow point shows  $d_{33}$  of the  $(\text{Bi}_{0.47}\text{Na}_{0.53})\text{TiO}_{2.97}$  sample with a close agreement to the trendline. In Fig. 7(b), meanwhile,  $d_{33}$  shows a linear decrease with increasing grain size with the exception of the  $(\text{Bi}_{0.47}\text{Na}_{0.53})\text{TiO}_{2.97}$  sample (hollow point) which shows a very low  $d_{33}$  but also a very small grain size. Considering these two figures together, it is evident that the most likely cause of the reduction in  $d_{33}$  is the composition changes rather than the grain size changes.

## B. Off-stoichiometric $(\text{Bi}_{0.5}\text{Na}_{0.5})\text{TiO}_3$

In order to confirm the hypothesis that the destruction of the piezoelectric properties of  $(\text{Bi}_{0.5}\text{Na}_{0.5})\text{TiO}_3$  is due to the compositional changes, two off-stoichiometric samples of  $(\text{Bi}_{0.5}\text{Na}_{0.5})\text{TiO}_3$  were prepared. The first sample, named the Na-poor sample, having a nominal composition  $[(\text{Bi}_{0.5}\text{Na}_{0.46})\text{TiO}_{2.98}]$ , was prepared so that the addition of 1 wt. %  $\text{Na}_2\text{CO}_3$  during sintering would result in a stoichiometric sample of  $(\text{Bi}_{0.5}\text{Na}_{0.5})\text{TiO}_3$ . The second sample, named the Na-rich sample, with a nominal composition of  $(\text{Bi}_{0.47}\text{Na}_{0.53})\text{TiO}_{2.97}$ , was produced to mimic the composition of the sample with the highest  $\text{Na}_2\text{CO}_3$  loading after sintering. This sample, thus, replicates the composition of that sample without the addition of  $\text{Na}_2\text{CO}_3$  during sintering, without the accompanying grain growth and also without the presence of  $\text{Bi}_2\text{O}_3$  precipitates. The microstructure, XRD patterns and piezoelectric properties of these samples were then analyzed to test the hypothesis that the destruction of the piezoelectric properties is due to compositional changes rather than microstructural effects.

## 4. XRD

The Rietveld refinement of the XRD pattern of the Na-rich sample [Fig. 8(a)] confirms the presence of single phase  $(\text{Bi}_{0.47}\text{Na}_{0.53})\text{TiO}_{2.97}$  with the change in composition leading to a significant reduction in the  $c$  parameter [from 13.5588(3) to 13.4431(2) Å] while the  $a$  parameter remains largely unchanged [5.4896(1) for the stoichiometric  $(\text{Bi}_{0.5}\text{Na}_{0.5})\text{TiO}_3$  and 5.4872(1) Å in the Na-rich composition]. These new unit cell parameters are in line with the changes observed in Bi deficient  $(\text{Bi}_{0.5}\text{Na}_{0.5})\text{TiO}_3$ <sup>32</sup> and are consistent with the replacement of  $\text{Bi}^{3+}$  by  $\text{Na}^+$  and the corresponding creation of oxygen vacancies. In the case of the Na-poor sample [whose Rietveld refinement is shown in Fig. 8(b)], a similar trend is seen in the unit cell parameters where the  $c$  parameter decreases from 13.5588(3) to 13.4620(4) Å, this time due to the creation of  $\text{Na}^+$  vacancies in the lattice. The XRD pattern also indicates the formation of  $\text{Bi}_2\text{O}_3$  to compensate for the Na sub-stoichiometry, leading to both Na and Bi vacancies. The unit cell parameters for both samples, along with those for stoichiometric  $(\text{Bi}_{0.5}\text{Na}_{0.5})\text{TiO}_3$  are summarized in Table IV below. The reduced unit cell parameters of the Na-rich sample are consistent with a lower bismuth content. The unit cell parameters for the Na-poor sample are reported after sintering with additional  $\text{Na}_2\text{CO}_3$ , the  $a$  parameter is in good agreement with that of the stoichiometric sample while the  $c$  parameter is slightly below the stoichiometric value, indicating that a small portion of the added  $\text{Na}_2\text{CO}_3$  was likely lost during sintering due to volatilization. The sample is thus still slightly deficient in Na ions.

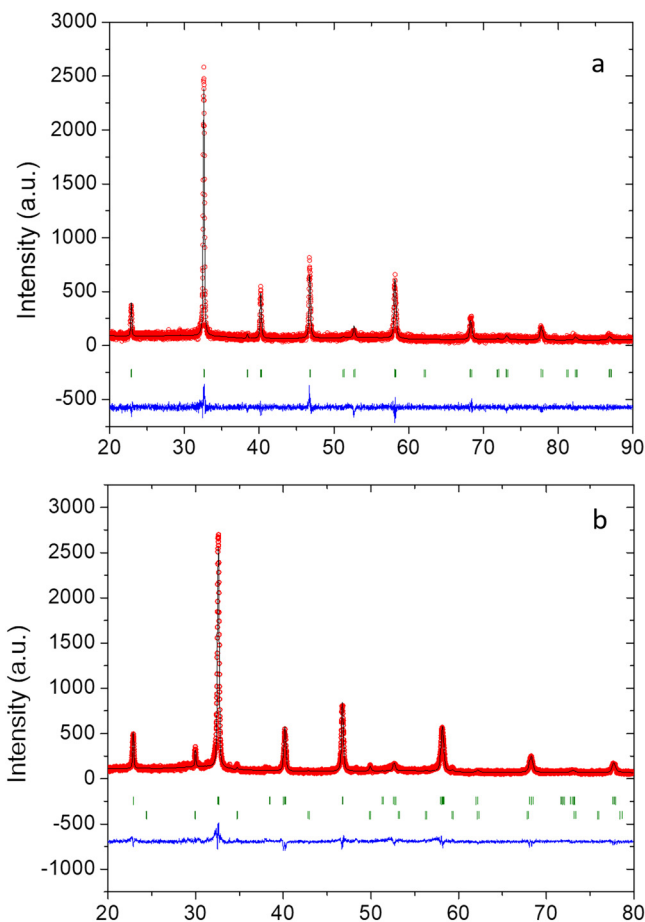


**FIG. 8.** Rietveld refinements of XRD data for (a) the Na-rich  $[(\text{Bi}_{0.47}\text{Na}_{0.53})\text{TiO}_{2.97}]$  and (b) the Na-poor  $[(\text{Bi}_{0.5}\text{Na}_{0.46})\text{TiO}_{2.98}]$  samples. For refinement b, the lower row of tick marks show the peak positions for cubic  $\text{Bi}_2\text{O}_3$ , while the other ticks denote the major phase.

## 5. Microstructure

Figure 9 shows the surface microstructure of both the Na-rich and Na-poor samples with a grain size  $\approx 1 \mu\text{m}$  in each case, slightly smaller but similar to the grain size of the stoichiometric  $(\text{Bi}_{0.5}\text{Na}_{0.5})\text{TiO}_3$  sintered without the addition of sintering aid. The

**TABLE IV.** Refined unit cell parameters of the off-stoichiometric  $(\text{Bi}_{0.5}\text{Na}_{0.5})\text{TiO}_3$  samples. The unit cell parameters for the Na-poor sample are after sintering with additional  $\text{Na}_2\text{CO}_3$ .

	Stoichiometric $(\text{Bi}_{0.5}\text{Na}_{0.5})\text{TiO}_3$	Na-Rich $(\text{Bi}_{0.47}\text{Na}_{0.53})\text{TiO}_{2.97}$	Na-Poor $(\text{Bi}_{0.5}\text{Na}_{0.46})\text{TiO}_{2.98}$
$a$ (Å)	5.4896(1)	5.4872(1)	5.4907(8)
$c$ (Å)	13.559(3)	13.443(2)	13.525(3)
$V$ (Å <sup>3</sup> )	353.8615	350.5352	351.4760

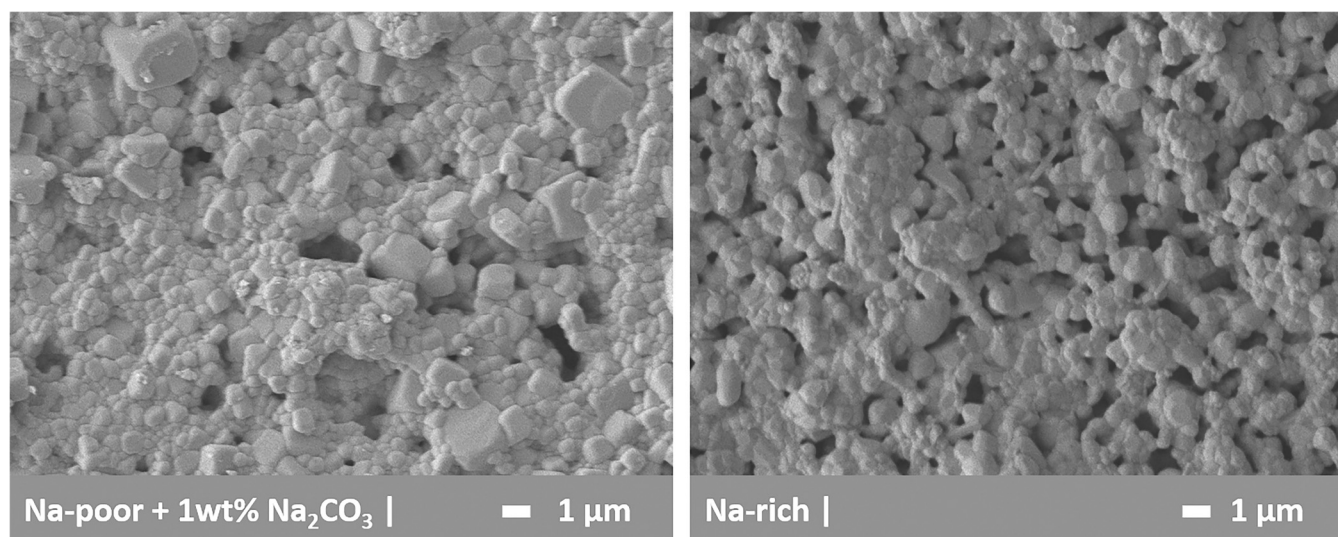


FIG. 9. SEM image of the surface microstructure Na-poor (left) and Na-rich (right) samples.

surface morphology of these samples was taken instead of the internal grain size because thermal etching did not sufficiently reveal the grain boundaries for reliable measurement. Thus, the surface grain size was taken as in Zuo *et al.*<sup>33</sup> It should, therefore, be noted that the internal grain size is expected to be slightly larger, as was observed for the stoichiometric sample. In the case of the Na-poor sample, this result is particularly interesting as 1 wt. %  $\text{Na}_2\text{CO}_3$  was added to reach stoichiometry during sintering. Based on the stoichiometric sample with the same  $\text{Na}_2\text{CO}_3$  loading, a grain size of approximately  $4\mu\text{m}$  is expected (Fig. 5). This allows us to investigate the addition of  $\text{Na}_2\text{CO}_3$  without modifying the composition or the grain size. One possible explanation for this difference is the change in the kinetics of  $\text{Na}_2\text{CO}_3$  uptake in the Na-poor case compared to the stoichiometric case. For the stoichiometric sample,  $\text{Bi}_2\text{O}_3$  precipitation from the lattice is observed during the sodium uptake. The kinetics of this precipitation in a sintering environment are likely slower than the uptake of Na alone, thus providing a bottleneck for the reaction speed that allows  $\text{Na}_2\text{CO}_3$  to continue to act as a sintering aid and grain growth agent for longer before its uptake. In the Na-poor case, Na and Bi vacancies are already present, thus allowing a faster  $\text{Na}_2\text{CO}_3$  uptake and limited grain growth. Small white spots are also visible in the SEM image for the Na-poor sample, which likely correspond to small amounts of residual  $\text{Bi}_2\text{O}_3$ . Unfortunately, due to their small size, this could not be verified with EDS measurements unlike the sample depicted in Fig. 6. Finally, the density of these pellets is seen to be similar to the stoichiometric case without the addition of  $\text{Na}_2\text{CO}_3$ . This microstructural similarity allows for an easy comparison of the effect of composition on the properties.

### 6. Piezoelectric properties

The off-stoichiometric samples were poled under the same conditions as the previous samples ( $100^\circ\text{C}$ ,  $4\text{ kV/mm}$ , 20 min). In

the Na-rich case, the sample presented a lower breakdown voltage and higher leakage currents attributed to induced ionic conductivity from the oxygen vacancies. Oxygen vacancies are expected for a  $(\text{Bi}_{0.5}\text{Na}_{0.5})\text{TiO}_3$  sample containing a high level of A-site vacancies to compensate for the charge imbalance. These types of defects have been shown to induce type I (oxide-ion driven) conductivity in  $(\text{Bi}_{0.5}\text{Na}_{0.5})\text{TiO}_3$  ceramics, especially those containing Bi sub-stoichiometry.<sup>15,34</sup> For this reason, the sample could not be exposed to fields in excess of  $2\text{ kV/mm}$  without breaking down and was thus poled at  $2\text{ kV/mm}$ . The piezoelectric properties of these samples have been summarized in Table V along with stoichiometric  $(\text{Bi}_{0.5}\text{Na}_{0.5})\text{TiO}_3$  for comparison. These data show that the Na-rich sample presents a drastically reduced  $d_{33}$  of only  $2.4\text{ pC/N}$ , in line with the observed changes in Table III for the samples with high  $\text{Na}_2\text{CO}_3$  loading. Furthermore, the grain size of around  $1\mu\text{m}$  is significantly below the grain size observed for the samples with  $\text{Na}_2\text{CO}_3$ , ruling out the impact of the grain size on the piezoelectric properties. Interestingly, the Na-poor sample (which should have achieved stoichiometry during the sintering process with added  $\text{Na}_2\text{CO}_3$ ) shows a  $d_{33}$  of  $40.1\text{ pC/N}$ . Considering that the unit cell parameters for this sample indicate that it still deviates slightly from stoichiometry, possibly due to  $\text{Na}_2\text{CO}_3$  volatilization during sintering, this lower value of  $d_{33}$  is expected. Large leakage currents were observed during the poling of this sample which are

TABLE V. Piezoelectric properties of pellets of  $(\text{Bi}_{0.5}\text{Na}_{0.5})\text{TiO}_3$  and the Na-rich and Na-poor variants.

	Stoichiometric $(\text{Bi}_{0.5}\text{Na}_{0.5})\text{TiO}_3$	Na-Rich $(\text{Bi}_{0.47}\text{Na}_{0.53})\text{TiO}_{2.97}$	Na-Poor $(\text{Bi}_{0.5}\text{Na}_{0.46})\text{TiO}_{2.98}$
$d_{33}$ (pC/N)	62.0	2.4	40.1

congruent with a small non-stoichiometry, leading to some ionic conduction while not high enough to cause a full breakdown of the sample at higher fields.

#### IV. CONCLUSIONS

In conclusion, while the addition of  $\text{Na}_2\text{CO}_3$  during the sintering step does result in improved densification and grain growth at lower temperatures than those usually used for sintering this ceramic, it also results in a drastic decrease in  $d_{33}$  of the system from 62 to 6 pC/N. This can be unambiguously linked to the compositional modifications that result from  $\text{Na}_2\text{CO}_3$  displacing Bi ions from the lattice, leading to a composition that is rich in Na ions and in the precipitation of  $\text{Bi}_2\text{O}_3$ . A reduction in  $d_{33}$ , driven mainly by the grain size effect, can be ruled out as the reproduction of the off-stoichiometric composition created by adding  $\text{Na}_2\text{CO}_3$  with a grain size around  $1\ \mu\text{m}$  still leads to the same reductions in  $d_{33}$ . This work represents a useful addition to the development of lead-free piezoceramics containing volatile elements by highlighting that while sintering aids can lead to improved densification at lower temperatures; they risk influencing the composition of the ceramic, altering its piezoelectric properties.

#### ACKNOWLEDGMENTS

During the preparation of this manuscript, Professor Groen tragically passed away. The remaining authors would like to thank him for his contribution in this work and many other works. He was a valued colleague and friend, and he will be greatly missed.

#### DATA AVAILABILITY

The data used in this study are available from the corresponding author upon reasonable request.

#### REFERENCES

- <sup>1</sup>A.G. Amelchenko, V.A. Bardin, V.A. VasiFev, V.D. Krevchick, P.S. Chernov, and M.A. Shcherbakov, in *2016 Dynamics of Systems, Mechanisms and Machines* (IEEE, 2016), pp. 1–4.
- <sup>2</sup>M. Chandrasekhar and P. Kumar, *Ceram. Int.* **41**, 5574 (2015).
- <sup>3</sup>S. E. Park and T. R. Shrout, *J. Appl. Phys.* **82**, 1804 (1997).
- <sup>4</sup>J. Rödel, W. Jo, K. T. P. Seifert, E. M. Anton, T. Granzow, and D. Damjanovic, *J. Am. Ceram. Soc.* **92**, 1153 (2009).
- <sup>5</sup>J. Rödel, K. G. Webber, R. Dittmer, W. Jo, M. Kimura, and D. Damjanovic, *J. Eur. Ceram. Soc.* **35**, 1659 (2015).
- <sup>6</sup>J. Ou-Yang, B. Zhu, Y. Zhang, S. Chen, X. Yang, and W. Wei, *Appl. Phys. A: Mater. Sci. Process.* **118**, 1177 (2015).
- <sup>7</sup>K. Pfeleiderer, R. Stoessel, and G. Busse, *Proc. SPIE* **5046**, 224 (2003).
- <sup>8</sup>Y. Zhang, X. Liu, G. Wang, Y. Li, S. Zhang, D. Wang, and H. Sun, *J. Alloys Compd.* **825**, 154020 (2020).
- <sup>9</sup>The European Parliament and the Council of the European Union, “Directive on the restriction of the use of certain hazardous substances in electrical and electronic equipment” (2011), pp. 88–110.
- <sup>10</sup>C. Sangsubun, *Ceram. Int.* **41**, S180 (2015).
- <sup>11</sup>Y. Saito, H. Takao, T. Tani, T. Nonoyama, K. Takatori, T. Homma, T. Nagaya, and M. Nakamura, *Nature* **432**, 84 (2004).
- <sup>12</sup>T. R. Shrout and S. J. Zhang, *J. Electroceramics* **19**, 111 (2007).
- <sup>13</sup>E. Taghaddos, M. Hejazi, and A. Safari, *J. Am. Ceram. Soc.* **97**, 1756 (2014).
- <sup>14</sup>Z. Li, H. Sun, X. Liu, H. Sui, and H. Guo, *Ceram. Int.* **46**, 11617 (2020).
- <sup>15</sup>F. Yang, M. Li, L. Li, P. Wu, E. Pradal-Velázquez, and D. C. Sinclair, *J. Mater. Chem. A* **6**, 5243 (2018).
- <sup>16</sup>V. R. Mudinepalli, S. H. Song, M. Ravi, J. Q. Li, and B. S. Murty, *Ceram. Int.* **41**, 6882 (2015).
- <sup>17</sup>M. Cernea, G. Poli, G. V. Aldica, C. Berbecaru, B. S. Vasile, and C. Galassi, *Curr. Appl. Phys.* **12**, 1100 (2012).
- <sup>18</sup>R. A. Dorey, S. A. Rocks, F. Dauchy, D. Wang, F. Bortolani, and E. Hugo, *J. Eur. Ceram. Soc.* **28**, 1397 (2008).
- <sup>19</sup>C. Chou, C. Liu, C. Hsiung, and R. Yang, *Powder Technol.* **210**, 212 (2011).
- <sup>20</sup>C. Chou, J. Chen, R. Yang, and S. Chou, *Powder Technol.* **202**, 39 (2010).
- <sup>21</sup>A. Watcharapasorn, S. Jiansirisomboon, and T. Tunkasiri, *Mater. Lett.* **61**, 2986 (2007).
- <sup>22</sup>K. R. Muhammed, A. Scrimshire, I. Sterianou, A. M. T. Bell, and P. A. Bingham, *J. Aust. Ceram. Soc.* **56**, 1441–1449 (2020).
- <sup>23</sup>L. Zhao, B. P. Zhang, W. Y. Wang, Y. H. Ding, S. M. Zhang, L. F. Zhu, and N. Wang, *Ceram. Int.* **42**, 7366 (2016).
- <sup>24</sup>G. O. Jones and P. A. Thomas, *Acta Crystallogr. Sect. B Struct. Sci.* **58**, 168 (2002).
- <sup>25</sup>Y. Hiruma, H. Nagata, and T. Takenaka, *J. Appl. Phys.* **105**, 084112 (2009).
- <sup>26</sup>Y. Hiruma, R. Aoyagi, H. Nagata, and T. Takenaka, *Jpn. J. Appl. Phys.* **44**, 5040 (2005).
- <sup>27</sup>C. Kornpom, T. Udeye, and T. Bongkarn, *Integr. Ferroelectr.* **177**, 59 (2017).
- <sup>28</sup>M. Spreitzer, M. Valant, and D. Suvorov, *J. Mater. Chem.* **17**, 185 (2007).
- <sup>29</sup>V. Buscaglia and C. A. Randall, *J. Eur. Ceram. Soc.* **40**, 3744–3758 (2020).
- <sup>30</sup>D. Damjanovic, *Rep. Prog. Phys.* **61**, 1267 (1998).
- <sup>31</sup>A. Sasaki, T. Chiba, Y. Mamiya, and E. Otsuki, *Jpn. J. Appl. Phys.* **38**, 5564 (1999).
- <sup>32</sup>X. Chen, J. Zeng, X. Yan, M. Zhou, P. Tang, T. Liang, and W. Li, *Solid State Ionics* **309**, 152 (2017).
- <sup>33</sup>R. Zuo, S. Su, Y. Wu, J. Fu, M. Wang, and L. Li, *Mater. Chem. Phys.* **110**, 311 (2008).
- <sup>34</sup>N. Bi, M. Li, M. J. Pietrowski, R. A. De Souza, H. Zhang, I. M. Reaney, S. N. Cook, J. A. Kilner, and D. C. Sinclair, *Nat. Mater.* **12**, 1 (2013).